Model-Based Iterative Reconstruction with a Gaussian Mixture MRF Prior for X-Ray CT

Ruoqiao Zhang, Debashish Pal, Jean-Baptiste Thibault, Ken D. Sauer, and Charles A. Bouman

***Abstract*—Markov random fields (MRFs) have been broadly used as prior models in tomographic reconstruction problems since they provide a simple and often effective way to model the spatial dependencies in images. However, due to the difficulty in parameter estimation, typical MRFs have very simple structures that may not fully capture various characteristics of complicated images. Recently, we developed a novel Gaussian mixture Markov random field (GM-MRF) model, which comprises a global image model by merging together individual Gaussian mixture models (GMM) for image patches. GM-MRF can capture complex image structures through patch GMMs, while the MRF parameters can be easily estimated using standard Gaussian mixture parameter estimation. In this paper, we apply GM-MRF as a prior model in model-based iterative reconstruction (MBIR). We present a novel analytical framework to calculate MAP estimates with a GM-MRF prior by using surrogate functions that lead to a sequence of quadratic optimizations. We demonstrate the value of the model with reconstructions of real clinical scans.**

***Index Terms*—Model-based iterative reconstruction, Markov random field, Gaussian mixture, patch-based model, prior model**

I. Introduction

Model-based iterative reconstruction (MBIR) algorithms have been widely applied to X-ray CT reconstruction problems [1]. MBIR algorithms typically incorporate an accurate system model, statistical noise model, and image prior model, which collectively improve image quality by reducing noise and improving resolution [2].

Finding good image priors is important for MBIR algorithms. The Markov random field (MRF) [3] has been one of the most popular choices of prior models in reconstruction problems. This model limits the dependencies in the image such that only local pixel interaction remains important. However, due to the difficulty in parameter estimation, MBIR algorithms typically use simple MRFs based on pair-wise interaction with a small number of parameters, which severely limits the expressiveness of the prior model. Recently, a more complex MRF model with implicit specification was used for CT reconstruction [4]; however, this model did not allow for explicit specification of the distribution of the whole image.

In recent years, there have been a number of efforts to improve the quality of priors through the use of more expressive models. In [5], Wang and Qi adapted a non-local prior model using as a mechanism to capture subtler image characteristics. A variety of research also adapted the ideas of dictionary learning to the problem of prior modeling in CT reconstruction [6]. More recently, there has been growing interest in modeling the multivariate distribution of the image using Gaussian mixture models (GMM). Since it is impractical to fit a single GMM to an entire image, most efforts have focused on modeling patches of the image with GMMs and then piecing together an integrated image model from the GMM patches. In [7] and [8], this approach was taken to modeling the image. However, the reconstruction method depends on the joint estimate of the image and the discrete GMM component for each patch. This discrete estimation process is essentially equivalent to the classification of each patch. However, erroneous patch classification has the potential to produce unwanted image defects. Moreover, accurate classification becomes problematic if a large number of GMM components are used to accurately model the patch characteristics.

Most recently, in [9] we proposed a method for creating a single integrated prior model of the entire image by seaming together GMM patch models using the geometric mean of the probability densities. This approach, which is similar to the product-of-experts technique [10], produces a single consistent probability density for the entire image. We call this integrated image model a Gaussian mixture Markov random field (GM-MRF). Importantly, we also derived an exact surrogate function for the GM-MRF's log likelihood function. This surrogate function allows for tractable minimization of the MAP function using a majorization-minimization approach. Moreover, this approach avoids the need to classify individual patches and allows for the use of much higher order GMM mixtures that can be more expressive.

In this paper, we incorporate a 3D GM-MRF prior model into X-ray CT reconstruction using MBIR. A major advantage of the GM-MRF model over existing prior models is that it allows for joint modeling of both the pixel intensities and spatial correlation. This is particularly important for CT reconstruction problems since the specific pixel values in such applications typically correspond to particular materials, each with their own distinctive spatial structure. Another important advantage is that the GM-MRF model is simple to train but expressive. In practice, it can be trained on high quality clinical images to capture real and important image characteristics, and the GM-MRF parameters can be easily estimated using standard methods for GMM parameter estimation such as the EM algorithm [11]. Each iteration of the reconstruction

This work was supported by GE Healthcare.

R. Zhang and C. A. Bouman are with the School of Electrical and Computer Engineering, Purdue University, West lafayette, IN 47907-0501 USA (email: zhang393@purdue.edu; bouman@ecn.purdue.edu).

D. Pal and J.-B. Thibault are with GE Healthcare Technologies, Waukesha, WI 53188 USA (email: debashish.pal@ge.com; jean-baptiste.thibault@med.ge.com).

K. D. Sauer is with the Department of Electrical Engineering, University of Notre Dame, Notre Dame, IN 46556-5637 USA (email: sauer@nd.edu).

algorithm computes a vector of soft classifications for each patch followed by a quadratic minimization step over the entire image. Our experimental results on low and high dosage CT scanner data indicate that the GM-MRF model can better render fine detail and edges in both high and low density regions of the reconstruction.

II. Proposed Algorithm

MBIR algorithms typically work by computing the maximum a posteriori (MAP) estimate given by

$$\hat{x} \leftarrow \arg\min_{x\in\Omega} \left\{ \frac{1}{2}\|y - Ax\|_{\Lambda}^2 - \log p(x) \right\}, \qquad (1)$$

where y is the measured data, and x is the unknown image. In this framework, the log-likelihood function $\frac{1}{2}\|y - Ax\|_{\Lambda}^2$ comprises the forward model of the measurement process, and the density $p(x)$ comprises the prior model for x, which will be discussed in detail in the following section.

A. Gaussian Mixture Markov Random Field (GM-MRF)

Let x be an image with pixels $s \in S$, where S is the set of all pixels in x. Let $P_s \in \mathcal{Z}^{p\times|S|}$ be a patch operator that extracts a p-dimensional patch at pixel s from the image. More precisely, P_s is a rank p matrix that has a value of 1 at locations belonging to the patch and 0 otherwise. Furthermore, we assume that each patch, $P_s x$, can be modeled as having a multivariate Gaussian-mixture distribution with K subclasses,

$$g(P_s x) = \sum_{k=0}^{K-1} \frac{\pi_k |B_k|^{\frac{1}{2}}}{(2\pi)^{p/2}} \exp\left\{ -\frac{1}{2}\|P_s x - \mu_k\|_{B_k}^2 \right\}, \qquad (2)$$

where parameters π_k, μ_k, B_k represent the mixture probability, mean, and inverse covariance of subclass k.

Then let $S_0, \cdots, S_{\eta-1}$ be a partition of the set of all pixels into η sets, each of which tiles the plane. In other words, $\{P_s x\}_{s\in S_m}$ forms a set of non-overlapping patches, which contains all pixels in x. Using this notation, we model the distribution of each tiling as the product of distributions of all its patches, as

$$p_m(x) = \prod_{s\in S_m} g(P_s x) = \exp\left\{ -\sum_{s\in S_m} V(P_s x) \right\}, \qquad (3)$$

where $V(P_s x) = -\log\{g(P_s x)\}$. In this case, $p_m(x)$ is a proper distribution that has the desired distribution for each patch. However, the discrete tiling of the plane introduces artificial boundaries between patches. To remove the boundary artifacts, we use an approach similar to the product-of-experts approach in [10] and take the geometric average of the probability densities for all η tilings of the plane to obtain the resulting distribution

$$p(x) = \frac{1}{z}\left(\prod_{m=0}^{\eta-1} p_m(x) \right)^{1/\eta} = \frac{1}{z}\left(\prod_{s\in S} g(P_s x) \right)^{1/\eta}, \qquad (4)$$

where z is a normalizing factor introduced to assure that $p(x)$ is a proper distribution after the geometric average is computed.

Therefore, we formulate a Gaussian mixture MRF (GM-MRF) model from (4) as

$$p(x) = \frac{1}{z}\exp\{-u(x)\}, \qquad (5)$$

with the energy function

$$u(x) = \frac{1}{\eta}\sum_{s\in S} V(P_s x), \qquad (6)$$

and the potential function

$$V(P_s x) = -\log\left\{ \sum_{k=0}^{K-1} \frac{\pi_k |B_k|^{\frac{1}{2}}}{(2\pi)^{p/2}} \exp\left\{ -\frac{1}{2}\|P_s x - \mu_k\|_{B_k}^2 \right\} \right\}. \qquad (7)$$

B. MAP Estimation with GM-MRF model

By substituting (5) into (1), we can calculate the MAP estimate with the GM-MRF prior as

$$\hat{x} \leftarrow \arg\min_{x\in\Omega} \left\{ \frac{1}{2}\|y - Ax\|_{\Lambda}^2 + u(x) \right\}. \qquad (8)$$

However, the second term in (8) is difficult for direct optimization due to the mixture of logarithmic and exponential functions. Therefore, we propose a functional substitution approach to replace this complex function with a mixture of quadratic functions that is computationally simpler to minimize.

For the function in (6), we define a quadratic function,

$$u(x; x') = \frac{1}{2\eta}\sum_{s\in S}\sum_{k=0}^{K-1} \tilde{w}_{s,k}\|P_s x - \mu_k\|_{B_k}^2 + c(x'), \qquad (9)$$

where x' represents the current state of the image,

$$\tilde{w}_{s,k} = \frac{\pi_k |B_k|^{\frac{1}{2}} \exp\left\{ -\frac{1}{2}\|P_s x' - \mu_k\|_{B_k}^2 \right\}}{\sum_{j=0}^{K-1} \pi_j |B_j|^{\frac{1}{2}} \exp\left\{ -\frac{1}{2}\|P_s x' - \mu_j\|_{B_j}^2 \right\}}, \qquad (10)$$

and $c(x')$ is only a function of the current state and therefore can be treated as a constant during optimization. Then it can be easily shown by using the lemma in [9],

$$u(x'; x') = u(x'), \qquad (11)$$

$$u(x; x') \geq u(x), \qquad (12)$$

which implies that $u(x; x')$ is a surrogate function for $u(x)$ so that majorization minimization methods can be used, and reduction of $u(x; x')$ ensures reduction of $u(x)$.

Therefore, the optimization in (8) can be implemented as a sequence of optimizations as

$$\text{repeat}\{ \quad \hat{x} \leftarrow \arg\min_{x} \left\{ \frac{1}{2}\|y - Ax\|_{\Lambda}^2 + u(x; x') \right\}$$
$$x' \leftarrow \hat{x} \quad \},$$

with one quadratic optimization problem at each iteration.

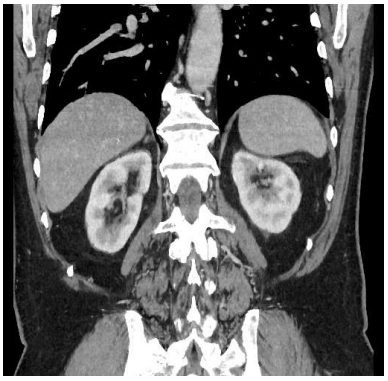

Fig. 1. Training data for 3D GM-MRF model: a normal-dose clinical CT reconstruction. Coronal view. Display window: window level (WL) 40 HU, window width (WW) 400 HU.

We use the iterative coordinate descent (ICD) algorithm [12] to solve this quadratic minimization problem. To do this, we solve the following 1D optimization problem for each pixel s,

$$\hat{x}_s \leftarrow \arg\min_{x_s \in \Omega} \left\{ \theta_1 x_s + \frac{1}{2}\theta_2 (x_s - x'_s)^2 + u(x_s; x'_s) \right\}, \quad (13)$$

with

$$u(x_s; x'_s) = \frac{1}{2\eta} \sum_{r \in \mathcal{S}_s} \sum_k \tilde{w}_{r,k} \| P_r x - \mu_k \|^2_{B_k} + c(x'), \quad (14)$$

where θ_1, θ_2 are the first two derivatives of the log-likelihood function [12] and S_s represents a set of pixels whose patches contain pixel s. This quadratic minimization problem can be solved exactly by any standard rooting algorithm.

III. Results

We train a 3D GM-MRF model consisting of 66 GMM subclasses for $5 \times 5 \times 3$ image patches, that is, a stack of 3 layers with a 5×5 patch at each 2D layer, by using the standard EM algorithm with the software in [11]. Training data contain 3×10^5 overlapping patches extracted from reconstructed images of a normal-dose clinical CT scan, which was collected on a Discovery CT750 HD scanner (GE Healthcare, WI, USA) in 64×0.625 mm helical mode, with 100 kVp, 312 mAs, 360 mm FOV, and pitch 1.375:1. Fig. 1 illustrates the 3D training images in the coronal view.

We apply the trained GM-MRF as a prior model in the MBIR algorithm. Experimental data was collected from the same patient as for the training data, with same scan setting except for a much lower dose level, which was 32 mAs. We compare the MBIR using GM-MRF prior with two other methods: FBP using a standard kernel, and MBIR using a traditional pair-wise MRF prior, the q-GGMRF model. Note that we intentionally reduced the regularization for MBIR with the q-GGMRF prior so as to obtain higher resolution, which lead to much higher noise as well.

Figs. 2, 3, and 4 present the comparison in different display windows and view planes. As compared to FBP, MBIR with GM-MRF prior produces images with sharper bones, more lung details, as well as less noise and streaks in soft tissues. When compared to MBIR with traditional q-GGMRF prior, as shown in Figs. 2 and 4, MBIR with GM-MRF prior reduces speckle noise in flat regions and along soft-tissue edges without impacting the edge definition. These improvements are due to better edge definition in the patch-based model over traditional pair-wise models. Moreover, Figs. 3 and 4 show that MBIR with GM-MRF prior reveals more fine structures and details in lung and bone regions. This indicates that the GM-MRF model is also a very flexible prior and inherently allows different regularization strategies for different anatomical regions in the CT images. This flexibility allows CT images with great soft-tissue quality and at the same time preserving the resolution in regions with larger variation, such as bone and lung.

IV. Conclusion

In this paper, we present a method for using GM-MRF priors in MBIR. The proposed method forms a global image model by merging together individual GMMs for image patches. In order to compute the MAP estimate using the GM-MRF prior, we use an exact surrogate function to make the optimization tractable. We compare the result with standard FBP as well as MBIR using a traditional pair-wise MRF prior in reconstruction experiments with high and low dosage clinical scans. The results demonstrate improved image quality.

References

[1] J.-B. Thibault, K. D. Sauer, J. Hsieh, and C. A. Bouman, "A three-dimensional statistical approach to improve image quality for multislice helical CT," *Med. Phys.*, vol. 34, no. 11, pp. 4526–4544, Nov. 2007.

[2] R. C. Nelson, S. Feuerlein, and D. T. Boll, "New iterative reconstruction techniques for cardiovascular computed tomography: how do they work, and what are the advantages and disadvantages?" *J. Cardiovascular Computed Tomography*, vol. 5, no. 5, pp. 286–292, 2011.

[3] J. Besag, "Spatial interaction and the statistical analysis of lattice systems," *Journal of the Royal Statistical Society. Series B (Methodological)*, pp. 192–236, 1974.

[4] P. Jin, E. Haneda, and C. Bouman, "Implicit Gibbs prior models for tomographic reconstruction," in *Signals, Systems and Computers (ASILOMAR), 2012 Conference Record of the Forty Sixth Asilomar Conference on*, 2012, pp. 613–616.

[5] G. Wang and J. Qi, "Penalized likelihood PET image reconstruction using patch-based edge-preserving regularization," *IEEE Trans. on Medical Imaging*, vol. 31, no. 12, pp. 2194–2204, 2012.

[6] Q. Xu, H. Yu, X. Mou, L. Zhang, J. Hsieh, and G. Wang, "Low-dose X-ray CT reconstruction via dictionary learning," *IEEE Trans. on Medical Imaging*, vol. 31, no. 9, pp. 1682–1697, 2012.

[7] D. Zoran and Y. Weiss, "From learning models of natural image patches to whole image restoration," in *Computer Vision (ICCV), 2011 IEEE International Conference on*, 2011, pp. 479–486.

[8] G. Yu, G. Sapiro, and S. Mallat, "Solving inverse problems with piecewise linear estimators: from Gaussian mixture models to structured sparsity," *IEEE Trans. Image Process.*, vol. 21, no. 5, pp. 2481–2499, 2012.

[9] R. Zhang, C. Bouman, J.-B. Thibault, and K. Sauer, "Gaussian mixture Markov random field for image denoising and reconstruction," in *Global Conference on Signal and Information Processing (GlobalSIP), 2013 IEEE*, Dec 2013, pp. 1089–1092.

[10] R. Salakhutdinov and G. Hinton, "An efficient learning procedure for deep Boltzmann machines," *Neural Computation*, vol. 24, no. 8, pp. 1967–2006, 2012.

[11] C. A. Bouman, "Cluster: An unsupervised algorithm for modeling Gaussian mixtures," April 1997, available from http://engineering.purdue.edu/~bouman.

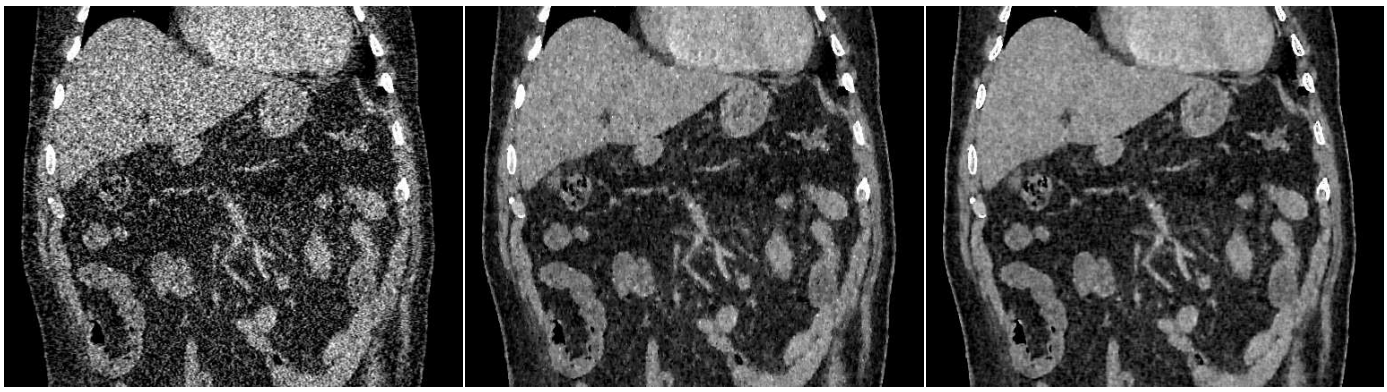

(a) FBP (b) MBIR w/ q-GGMRF w/ reduced regularization (c) MBIR w/ GM-MRF prior

Fig. 2. Comparison between different reconstruction methods and models with low-dose data. Coronal view. Display window: WL 40 HU, WW 400 HU. The result of MBIR with q-GGMRF prior was produced with reduced regularization so as to obtain higher resolution, which lead to higher noise as well.

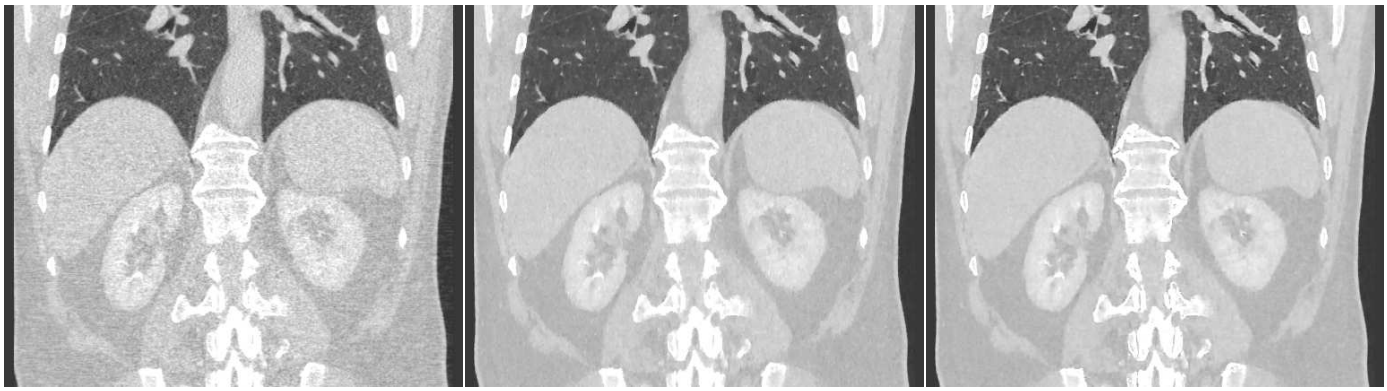

(a) FBP (b) MBIR w/ q-GGMRF w/ reduced regularization (c) MBIR w/ GM-MRF prior

Fig. 3. Comparison between different reconstruction methods and models with low-dose data. Coronal view. Display window: WL -500 HU, WW 1800 HU. The result of MBIR with q-GGMRF prior was produced with reduced regularization so as to obtain higher resolution, which lead to higher noise as well.

(a) FBP (b) MBIR w/ q-GGMRF w/ reduced regularization (c) MBIR w/ GM-MRF prior

Fig. 4. Comparison between different reconstruction methods and models with low-dose data. Axial view. Display window: WL 40 HU, WW 400 HU. The result of MBIR with q-GGMRF prior was produced with reduced regularization so as to obtain higher resolution, which lead to higher noise as well.

[12] K. D. Sauer and C. A. Bouman, "A local update strategy for iterative reconstruction from projections," *IEEE Trans. on Signal Processing*, vol. 41, no. 2, pp. 534–548, Feb. 1993.